Journal of
Applied Crystallography
ISSN 0021-8898

Received 12 January 2010
Accepted 17 May 2010

Diamond plates on dome-like particles: preparation, characterization and field emission properties

Rajanish N. Tiwari,* Wei-Chun Chen, Jitendra N. Tiwari, Wei-Lin Wang and Li Chang

Department of Materials Science and Engineering, National Chiao Tung University, Hsinchu, 300, Taiwan. Correspondence e-mail: rajanisht@gmail.com

Thin diamond microplates have been grown on dome-like/hemispherical carbon particles on titanium carbide by a microwave plasma chemical vapour deposition (MPCVD) method using a gas mixture of methane and hydrogen. The diamond microplates have a thickness of about 200 nm. A thin (300 nm) film of titanium carbide was formed during carburization of sputtered titanium on an Si(100) substrate in MPCVD. The hemispherical carbon particles were covered with diamond microplates. The diamond microplates are isolated electron-emitting spherules and exhibit a low threshold (50 V μm^{-1}) and high current density (0.92 mA cm^{-2}) in their field emission properties. A possible mechanism for the formation of the diamond microplates and hemispherical carbon particles is presented.

1. Introduction

Recently, the synthesis of diamond particles with particular shapes has received much attention because of the excellent properties of diamond, such as its wide band gap, high thermal conductivity and chemical inertness, excellent biological compatibility, superior hardness, optical transparency, and high carrier mobility. These outstanding properties of diamond give it a wide range of applications, for instance in optics, microelectronics, tribology, thermal management, biomedicine, DNA sensors and so on (Tiwari *et al.*, 2010; Yan & Chang, 2006; Tiwari & Chang, 2010*a*,*b*). Previous studies have shown that diamond crystallites have been synthesized by chemical vapour deposition in a variety of forms, such as polyhedra, powders, platelets and cauliflower-like particles, in the size range from nanometres to micrometres (Yan & Chang, 2006; Guo & Chen, 2007; Bakowicz-Mitura *et al.*, 2007; Chen & Chang, 2004).

The particular shape of the diamond particles is believed to be vitally significant for the development of technological applications. It has been predicted that diamond nanorods may have unusual mechanical properties (Shenderova *et al.*, 2003). There have also been some reports of the fabrication of diamond crystals with octahedral, decahedral and cuboctahedral morphologies, which are highly faceted with sharp corners and edges, and of multiply twinned diamond crystals. Several authors have attempted to fabricate diamond nanopillars or nanowhiskers, either by plasma etching or by growth on anodic aluminium oxide templates (Chen *et al.*, 2008). Lu & Chang (2004, 2005) reported regular {110} and {111} hexagonal diamond nanoplatelets, and recently Chen & Chang (2009) also noticed that nanocrystalline vertical diamond in a platelet configuration has a hexagonal shape. The formation of diamond platelets is due to defects in twinned crystals. Vlasov *et al.* (2007) produced hybrid diamond–graphite nanowires by microwave plasma chemical vapour deposition (MPCVD), consisting of a single crystalline diamond core oriented along the ⟨110⟩ principal axis covered with graphite shells of different thicknesses. These kinds of diamond shapes may show different physical and chemical properties because of their intrinsic structural characteristics. Thus, the growth of a unique morphology of diamond is not only an experimental challenge but also has theoretical significance. In addition, most of the properties of diamond plates have not been investigated fully, with the majority of studies to date being concentrated on theoretical predictions and the corresponding experimental studies still at an early stage.

In the present study, we report a simple and efficient method for the deposition of a well ordered structure of thin diamond plates on dome-like or hemispherical carbon particles by MPCVD using a mixture of CH_4 and H_2 gases. The deposited diamond plates, of micrometre size, exhibit the appearance of facets. Their excellent field emission properties are also reported. Titanium carbide was used as the buffer layer, because titanium and its carbide buffer layer not only prevent carbon from diffusing deeply into the substrate but also develop strong chemical bonding to increase adhesion (Guo & Chen, 2007; Grogler *et al.*, 1997).

2. Experimental details

The synthetic process for the diamond plates is described as follows. Mirror-polished *p*-type (100) silicon wafers with

Table 1
MPCVD experimental parameters for each process.

System parameter	H_2 plasma clean	Carburization	Bias for diamond nucleation	Diamond growth
CH_4 (%) in H_2		5.6	1.7	2.6
H_2 (s.c.c.m.)	300	300	300	300
Power (W)	600	600	900	900
Pressure (Torr)	25	20	30	30
Temperature (K)	918	913	1223	1223
Negative bias (V)	75	75	100	
Bias time (min)	1	10	10	
Growth time without bias (min)	22	120		135

dimensions of 1 × 1 cm were used as substrate without any mechanical pre-treatment. The substrates were ultrasonically cleaned in acetone and methanol for 10 min each, and then high-pressure N_2 gas was used to remove any remaining particles from the Si surface. The cleaned samples were dipped into a buffered oxide etch solution (specific composition 5% HF in deionized water) for 5 min to remove the native oxide layer from the Si surface. The cleaned Si substrate was then placed on an Mo disc holder for deposition of the titanium (Ti) film. A Ti target (99.999% purity) was used in a radio-frequency (RF) magnetron sputtering system at 200 W. After being evacuated to a base pressure of 1×10^{-6} Torr (1 Torr = 133.322 Pa), the working chamber was filled with Ar (99.99% purity), with a constant Ar gas flow of 10 standard cubic centimetres per minute (s.c.c.m.) throughout the deposition process. The sample was prepared at 573 K with a typical working pressure of 1 mTorr.

The sputtered Ti/Si substrate was then ultrasonically cleaned with acetone and methanol for 10 min each, and placed on an Mo disc holder for carburization and diamond growth, which was carried out in an AsTeX-type MPCVD system. Once loaded into the MPCVD system, the substrate was cleaned with hydrogen plasma at a DC bias voltage of −75 V for 1 min, and then for another 22 min without bias. For carburization of the Ti/Si substrate, we used 5.6% CH_4 in H_2 and a bias voltage of −100 V for 10 min, followed by further deposition for 2 h without bias on the sample (details in Table 1). After carburization, we used hydrogen plasma with the addition of 1.7% CH_4 and a bias voltage of −100 V for 10 min to enhance the nucleation. For diamond growth on the TiC/Si substrate, we removed the bias and increased the CH_4 concentration to 2.6% for ∼135 min (details in Table 1).

The surface morphology of the sample was examined using field-emission scanning electron microscopy (SEM; JEOL JSM-6700F) and the chemical composition of the surface was characterized by X-ray photoelectron spectroscopy (XPS; Thermo VG 350F, Mg *Kα* X-ray source). Elemental mapping in cross section was performed using a PHI700 scanning Auger nanoprobe (ULVAC-PHI Inc.). Examination of the internal microstructures of the deposited materials was carried out using transmission electron microscopy (TEM; Philips Tecnai20 operated at 200 kV). The cross-sectional TEM specimen was prepared using a focused ion beam (FIB; FEI Nova 200 dual-beam FIB). For the protection of the TEM specimen against damage from the high-energy ion beam (30 keV Ga^+), the specimen was coated with platinum. Raman spectroscopy was performed using a LABRAM HR800 system with an Ar laser (wavelength 514.5 nm), which could be focused to ∼1 µm diameter for micro-mode operation. The crystallinity of the diamond was evaluated using an X-ray diffractometer (Siemens D5000).

The field emission measurements were carried out in a vacuum chamber with a base pressure of 10^{-6} Torr at room temperature using a parallel cathode–anode setup (Lee *et al.*, 2005), with a 1 mm-diameter molybdenum tip as anode. The distance between the anode tip and the cathode was controlled at 10 µm by a digital micrometer controller and an optical microscope. The current–voltage characteristics of the films were acquired using a Keithley 237 electron source unit and modelled using the Fowler–Nordheim theory (Fowler & Nordheim, 1928).

3. Results and discussion

The structure, surface morphology and size of the synthesized diamonds were examined using SEM. The top-view and cross-sectional SEM images in Figs. 1(*a*) and 1(*b*), respectively, show that, after carburization of a 200 nm sputtered Ti film on Si for 120 min, many hemispherical particles have been synthesized on the Ti/Si(100) substrate surface with an approximate density of 2.4×10^7 cm^{-2}. They are either isolated, with a perfect spherule shape, or coalesced together into irregular shapes. The average diameter and height of the deposited carbon particles are ∼6 and ∼5.6 µm, respectively. The carbon particles might be similar to the cauliflower diamond crystallites often observed in the case of deposition with a high CH_4/H_2 ratio. After diamond growth for 135 min, disc-like diamond microplates are found to be deposited all over the surface of

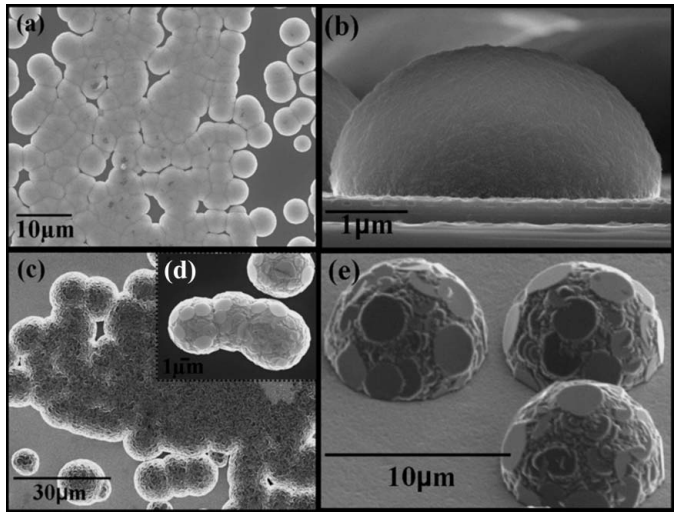

Figure 1
SEM images showing the surface morphology of the deposited particles on the substrate after carburization of Ti/Si. (*a*) Top view and (*b*) cross-sectional view. (*c*)–(*e*) SEM images after diamond growth, (*d*) top view and (*e*) angled view.

each hemispherical carbon particle, as shown in Figs. 1(*c*) and 1(*d*). As a result, the hemispherical carbon particles are transformed into dome-like particles covered with faceted plates. The identification of the diamond phase is shown in the TEM and XRD data. The disc-like diamond microplates have a size of a few micrometres. From these images, it can be seen that the diamond microplates exhibit a smooth surface morphology on the hemispherical carbon particles. The relatively high density of particles with a hemispherical morphology obtained on Ti/Si without pretreatment is reasonable, as Ti is a strong carbide-forming element which can promote diamond nucleation with a high concentration of methane (Guo & Chen, 2007; Silva *et al.*, 2002). Another reason may come from the assistance of bias to enhance nucleation at the carburization stage.

After carburization of the sputtered continuous ~200 nm Ti film on the Si substrate, XPS characterization shows that titanium carbide (TiC) has formed, as shown in Fig. 2. As can be seen in Fig. 2(*a*), two carbon peaks are located at about 281.7 and 284.7 eV. The weak peak at 281.7 eV can be assigned to carbon in the carbide state, which is characteristic of Ti—C bonding, while the other broad peak at 284.7 eV can be attributed to graphitic carbon (Hogberg *et al.*, 2001). The Ti 2*p* region displays two dominant peaks centred at ~460.6 and ~455.0 eV, representative of the $2p^{1/2}$ and $2p^{3/2}$ peaks of TiC (Perry *et al.*, 1993).

The crystallographic and microstructural characterization of the plates formed after diamond growth was carried out on a cross-sectional TEM specimen prepared by the focused ion beam method. A typical cross-sectional bright-field TEM (BF-TEM) image of diamond/TiC/Si is shown in Fig. 3(*a*), from which it is clear that both the TiC interlayer (thickness ~300 nm) and the carbon particles have been formed on the Si substrate. The enlarged view in Fig. 3(*b*) illustrates the microstructure of the hemispherical carbon particles deposited on the TiC. The selected area diffraction (SAD) pattern in Fig. 3(*c*) from the interlayer region mainly shows a typical ring pattern (from inner to outer), corresponding to the TiC {111}, {200}, {220} and {311} planes formed on the Si substrate and without any observation of metallic Ti diffraction reflections, suggesting that the 200 nm-thick Ti film reacted with carbon to form TiC after carburization for 120 min in MPCVD. The SAD pattern in Fig. 3(*d*) shows the diamond {111}, {220} and {311} rings, implying that the diamond particles are probably formed during the growth of hemispherical carbon particles after carburization. From image-contrast and microdiffraction patterns, it can be shown that the carbon particle is actually an amorphous phase (a mixture of amorphous carbon and diamond in major and minor fractions, respectively). The dark-field image in Fig. 3(*e*), taken from a {111} diamond diffraction spot in Fig. 3(*d*), shows that there are many small diamond particles of ~10 nm located along the directions of radial growth from the centre and at the interface of the hemispherical particle with the substrate. The distribution of these particles implies that they may be co-deposited with amorphous carbon and incorporated within the hemispherical carbon particles. This could occur as a result of the bias effect caused by the high CH_4 concentration of 5.6% during the carburization stage. Once the hemispherical carbon particles have been formed, one can observe the diamond plates synthesized on top of them in the growth stage. The SAD

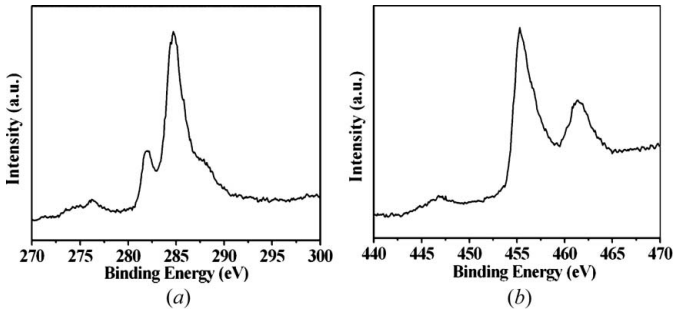

Figure 2
XPS spectra of the (*a*) C1 *s* and (*b*) Ti 2*p* peaks for deposited films of TiC.

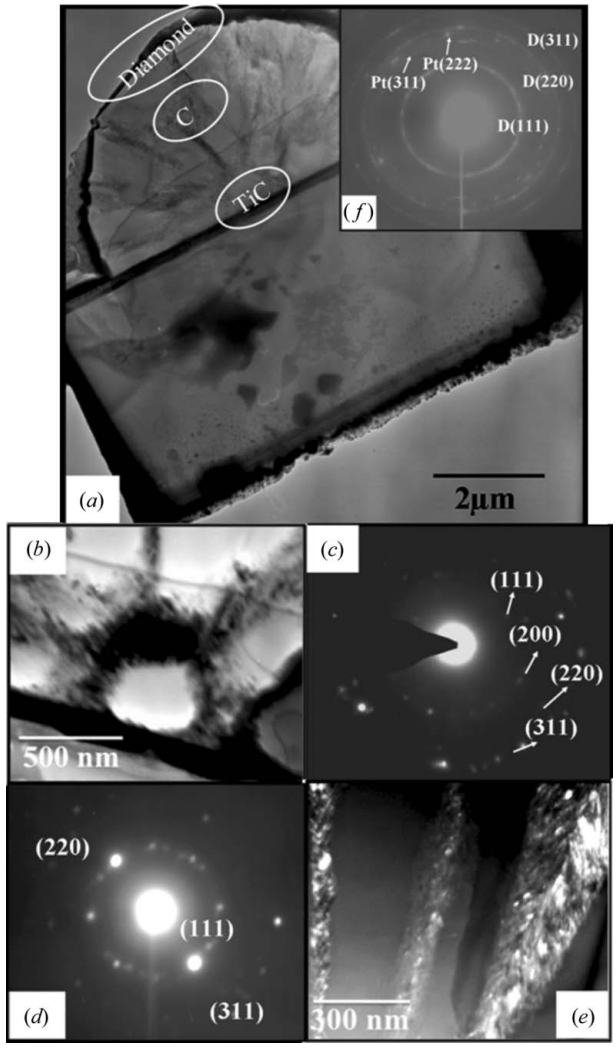

Figure 3
(*a*) Cross-sectional BF-TEM image of diamond/TiC/Si. (*b*) Enlarged BF image of marked area around interfacial regions of carbon particle/TiC. (*c*) SAD pattern from the crystalline TiC interlayer. (*d*) SAD pattern from the region labelled C inside the hemispherical carbon particle. (*e*) Dark-field image taken from a diamond diffraction spot. (*f*) SAD pattern of diamond deposited on top of the hemispherical carbon particle.

pattern from the top region in Fig. 3(*f*) shows a typical ring pattern (from inner to outer), corresponding to the diamond {111}, {220} and {311} planes, in addition to the Pt {311} and {222} rings, due to the Pt coating applied to protect the TEM specimen against ion damage in the FIB. In general, the presence of multiply twinned crystals (intergrowth of two separate crystals in a variety of specific configurations) may result in the formation of diamond plates. Previous studies have shown that diamond platelets have been formed as a result of twinned crystallite formation. Chen & Chang (2009) proposed that the twin lamellae are parallel to the platelets and the main tabular planes of the diamond nanoplatelets are the {111} planes. The growth of diamond nanoplatets through the {100}/{111} side faces adjacent to the twinned planes provides preferential sites for the nucleation of new layers (Chen *et al.*, 2008; Lu & Chang, 2004, 2005). Thus, we believe that, if we carry out further analysis at atomic resolution, we may find that the diamond plates are also formed as a result of the presence of multiple twinned crystalline particles along with other structural defects (Yacoot *et al.*, 1998; Machado *et al.*, 1998). The thickness of the diamond plates on the carbon hemispheres is ∼200 nm on average.

We used Auger electron mapping in a cross-sectional view to identify the presence of elements and their distribution on the surface after diamond growth. The cross-sectional specimen was prepared simply by cleavage. Fig. 4 shows a SEM micrograph in a cross-sectional view, with the corresponding maps of C, Ti and Si. From the image contrast in the SEM and elemental maps, one can clearly identify three regions which correspond to the carbon, TiC and Si phases. The thickness of the TiC interlayer is ∼0.3 µm, consistent with TEM observations, while the hemispherical carbon particle on the TiC/Si substrate has a height of about ∼6 µm. Since no other interlayer can be observed, this may verify that the Ti buffer layer sputtered on the Si substrate has almost reacted with carbon to form the TiC layer, as suggested by the TEM results. Observation of the TiC interlayer with diamond and Si may suggest that the TiC has survived in the bias-enhanced nucleation (BEN) and growth stages of diamond deposition without being etched away, and can thus protect the Si substrate below from etching, which has often been observed after BEN treatment for diamond deposition. It also seems that the micrometre-sized carbon hemisphere might be directly formed on the TiC/Si substrate during carburization.

The evidence for synthesized diamond is supported by micro-Raman spectra, as shown in Fig. 5. After carburization of Ti/Si, Fig. 5(*a*) obtained from a dense area of a number of hemispherical carbon particles shows Raman peaks at 1120, 1348 and 1601 cm^{-1}. The Raman peaks at 1348 and 1601 cm^{-1} are the *D* and *G* bands of sp^2 bonding, respectively. The *G* peak is due to the E_{2g} graphite mode, while the *D* mode is related to disordered graphitic-like sp^2-bonded carbon. The origin of the peak at 1120 cm^{-1} is not well understood in terms of bonding characteristics, but it is often observed in Raman spectra of nanocrystalline diamond films (Sharda *et al.*, 2001; Lin *et al.*, 2000; Fayette *et al.*, 1998). Previous studies have shown that the peak at 1120 cm^{-1} usually appears for diamond nanocrystals of 1–2 nm in diameter or carbon clusters of sp^3-bonded material (Nemanich *et al.*, 1988; Sowers *et al.*, 1999). Thus, it is likely that nanostructured diamond particles may

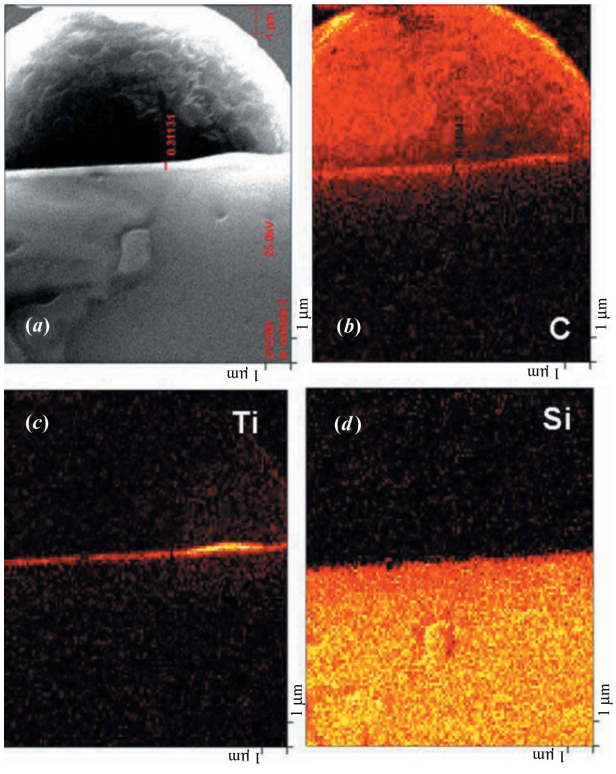

Figure 4
(*a*) Cross-sectional SEM of deposited diamond/TiC/Si, with the corresponding nanobeam Auger electron mapping of (*b*) carbon, (*c*) titanium and (*d*) silicon.

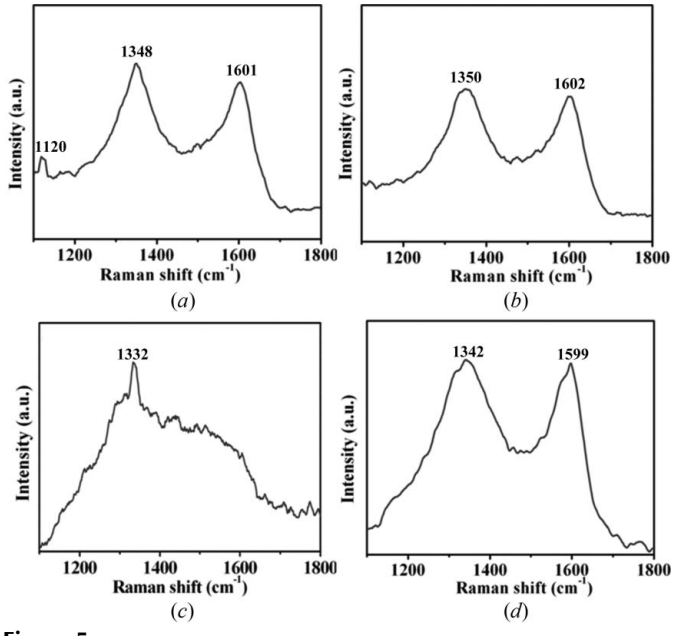

Figure 5
Raman spectra (*a*) from a hemispherical particle, (*b*) from a region without particles after carburization, (*c*) from a diamond microplate on a hemispherical particle and (*d*) from a region without particles after diamond growth.

form with sp^2 carbon after carburization in the present case. After the carburization stage, the resulting morphology seems to be a cauliflower shape. A sharp Raman peak at 1332 cm^{-1} from a cauliflower diamond shape has been reported previously (Park *et al.*, 1994; Buijnsters *et al.*, 2003), while we did not observe such a peak after carburization, as shown in Fig. 5(*a*). From the Raman spectra, it is clear that the structural morphology (Figs. 1*a* and 1*b*) is similar to a cauliflower diamond shape but indeed it is not a cauliflower diamond. This is supported by our TEM observations in Fig. 3. The Raman spectrum from a surface region without hemispherical particles only shows peaks at 1350 and 1602 cm^{-1}, corresponding to *D* and *G* bands, as shown in Fig. 5(*b*). After diamond growth, the Raman spectra shown in Figs. 5(*c*) and 5(*d*) are obtained from the dome-like particles and a region without coverage of dome-like particles, respectively. In Fig. 5(*c*), it is clearly seen that the highest intensity peak at 1332 cm^{-1} is characteristic of diamond, while Fig. 5(*d*) only shows a very small diamond peak at 1332 cm^{-1}, with strong *D* and *G* bands at 1342 and 1599 cm^{-1}, respectively. It is evident that the diamond is mainly deposited as discs on the hemispherical carbon particles. In addition, the existence of TiC and diamond is evident from the XRD measurements. XRD data were analysed in order to identify the crystal structure and the various phases present in the sample. Fig. 6 shows a typical XRD pattern from a sample after diamond growth. It clearly shows the TiC (111) and (200) peaks as well as the diamond (111) peak, consistent with the results mentioned above. The average size of the diamond platelets/particles was calculated using the Debye–Scherrer equation, given by

$$d = 0.9\lambda/\beta\cos\theta, \qquad (1)$$

where d is the average size of the particles, λ is the wavelength of the radiation used, β is the full width at half-maximum in radians and θ is half of the scattering angle (Roy *et al.*, 2009). It seems that some nanocrystalline diamond particles have also been formed with diamond plates on the dome-like carbon particles. Therefore, we note that the average crystallite size of the diamond plates/particles is ~602 nm with an error of ±1 nm.

After diamond growth, the field emission properties were investigated. Fig. 7 shows the relation of emission current density as a function of applied electrical field for both dome-like particles and a continuous diamond film. A comparison of the field emission characteristics of the two samples was carried out by defining the threshold field ξ_{th} corresponding to a current density of 10 μA cm^{-2}. The inset in Fig. 7 is the corresponding Fowler–Nordheim (F–N) plot, $\ln(J/E^2)$ *versus* $1/E$, of the corresponding field emission (FE) data, indicating that the field electron emissions of both dome-like particles and a continuous diamond film follow the classic field emission mechanism. The turn-on field of the diamond plates at a current density of 0.013 mA cm^{-2} is approximately 50 V μm^{-1}, which is much less than that of a continuous diamond film (turn-on field for a diamond film at a current density of 0.0012 mA cm^{-2} is 69 V μm^{-1}). The field at an emission current density of 1 mA cm^{-2} is about 76 V μm^{-1}, which compares favourably with various microstructured film emitters. The field at which an emission current density of 0.92 mA cm^{-2} is achieved is considered a figure of merit for conventional flat panel displays, as well as for a continuous diamond film (0.13 mA cm^{-2} at 98 V μm^{-1}). The value for the present system is less than 90 V μm^{-1}, which is better than previously reported values for various field emitting materials including microdiamond films (Arora & Vankar, 2006), but worse than those of oriented nano-, submicro- and microdiamond films. For these films, Wang *et al.* (2002) noticed higher current densities of 780, 300 and 180 μA cm^{-2} for applied voltages of 1.5, 10 and 25 V μm^{-1}, respectively. The SEM image in Fig. 1(*d*) shows that well ordered diamond plates have been formed on the hemispherical shape, although some have coalesced together and formed well ordered edge plates. It may be that these edges can act as electron emitters,

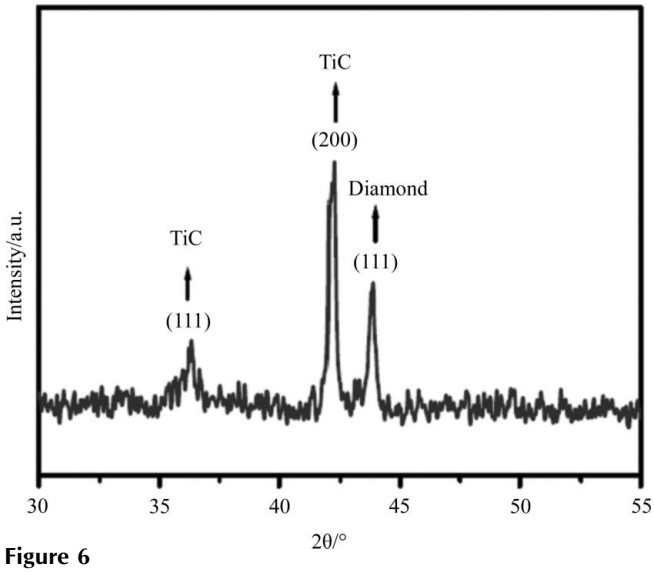

Figure 6
X-ray diffraction pattern of a sample after diamond growth, showing diamond and TiC peaks.

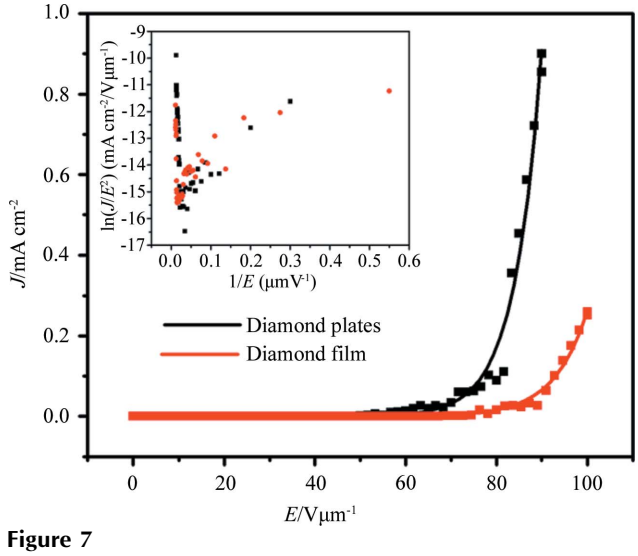

Figure 7
Emission current density as a function of applied electric field for diamond plates and film. Inset: corresponding F–N plot.

resulting in a high current density of 0.92 mA cm^{-2} with an applied field of 81 V μm^{-1}. For continuous microdiamond films with a surface morphology of irregular edges, the resultant high current density is 0.13 mA cm^{-2} at 98 V μm^{-1}.

The low turn-on field and high current density of diamond plates on hemispherical particles may be assigned to the following factors. Firstly, the well faceted edges (Figs. 1*c* and 1*d*) may enhance the field emission properties (Chen & Chang, 2009). Secondly, diamond plates on a hemispherical shape may act as separate emitting edges, which may not only have a large field-enhancement factor but also effectively depress the screen effect. Finally, the deposited sp^2-bonded carbon materials in a region without hemispherical particles (Raman spectrum in Fig. 5*d*) may also influence the field emission properties (Carey *et al.*, 2000; Burden *et al.*, 1999). A continuous diamond film (not shown here) has an irregular facet morphology with little non-diamond carbon, implying that it has a high resistivity for electron emission, because it is difficult for electrons to travel through irregularly faceted bulk diamond. Therefore, an irregular diamond film has very low field emission properties compared with diamond plates with well ordered facets. Davidson, Kang and co-workers have demonstrated the good field emission properties of diamond microtips (Kang *et al.*, 1996; Davidson *et al.*, 2003; Kang, Davidson, Wisitsora-at *et al.*, 2004; Kang, Davidson, Wong & Holmes, 2004). Further study of diamond plates (*e.g.* to produce unique diamond shapes by patterning and etching) may yield not only excellent field emission properties but also other potential applications. Besides field emission applications, horizontal/vertical diamond plates have been used in biosensors, nanoelectronics, fuel cells, micromachine elements and so on (Chen & Chang, 2004; Chen *et al.*, 2008; Vlasov *et al.*, 2007; Noguchi *et al.*, 2003). Previous studies have shown that diamond platelets are formed with a graphite layer (Chen & Chang, 2004; Vlasov *et al.*, 2007). If we etch these few layers of graphite then graphene will be formed. It is well known that graphene has a wide range of applications (Wang *et al.*, 2008; Stoller *et al.*, 2008; Mohanty & Berry, 2008; Schedin *et al.*, 2007; Novoselov *et al.*, 2004).

In this study, micro-sized diamond plates have been synthesized with a unique morphology. Previous CVD studies have shown that diamond can be synthesized in a variety of shapes, such as polyhedra, powders, platelets and cauliflower-like particles, in the size range from nanometres to micrometres (Guo & Chen, 2007; Bakowicz-Mitura *et al.*, 2007; Chen & Chang, 2004; Yan & Chang, 2006). The typical shape, surface morphology and internal structure of the hemispherical carbon particles may provide some essential information to understand the growth mechanisms. After carburization of Ti/Si, carbon particles on the substrate probably coexist with diamond crystallites, as shown by cross-sectional TEM.

In a microwave plasma, a mixture of methane and hydrogen gases can produce hydrogen and methyl radicals (CH_3^*), as shown in the reaction

$$CH_4 + H^* \rightarrow CH_3^* + H_2. \qquad (2)$$

H-atom abstraction from the CH_4 molecules may also form other active hydrocarbons which are readily adsorbed, coalesced or decomposed on the Ti/Si surface and form the titanium carbide layer (Chen *et al.*, 1998; Nagai *et al.*, 2008; Liu *et al.*, 2003). A clean Ti/Si surface may be composed of only Ti and oxygen, which often form a 2–5 nm oxide monolayer on the outermost surface. Since the Ti surface was free of any other foreign particles, a pure hydrogen plasma (300 s.c.c.m. H_2 flow) was used to clean the Ti/Si surface, removing the oxide layer and any contaminants from the surface. Such plasma-cleaned surfaces can be highly active, which may promote the reaction of C atoms and/or ions with titanium to form a titanium carbide interlayer on the Ti/Si surface. During carburization with a negative bias on the substrate, positively charged ions accelerate toward the Ti/Si substrate and may further enhance the reaction of carbon with the Ti surface for the formation of titanium carbide.

After reaction for a short time, excess carbon species from the high methane concentration of 5.6% may form hemispherical carbon particles. Since a negative bias was applied to the substrate during carburization, it is likely that the surface energy has been modified, leading to the formation of a hemispherical shape. Also, it is well known that bias can enhance diamond nucleation, which may explain why nanodiamond crystallites exist within the carbon particles. The fan-out characteristic of the nanodiamond distribution in a hemispherical particle, from the centre of the particle at the interface between the particle and the TiC interlayer, probably suggests that these nanodiamonds act as nucleation sites for diamond microplate formation. A similar observation of diamond deposition on an Si substrate has been reported previously (Williams & Glass, 1989).

It is well known that a hydrogen plasma preferentially etches the non-diamond phase. Probably, with a longer treatment time in MPCVD the non-diamond carbon phase is either etched or converted into relatively stable sp^3-bonded carbon in a gaseous plasma (CH_4 and H_2).

A possible growth mechanism for the formation of diamond plates on the synthesized hemispherical carbon particles is briefly discussed. In general, the high substrate temperature and low methane concentration have been shown to favour diamond formation. The curved shape of the carbon particles has a high surface activity, providing more roughened surface sites for diamond formation. This implies that hydrogen chemisorption on a curved region is easier than on a planar graphite surface, so a rehybridization of the carbon from sp^2 to sp^3 can be energetically more favourable than a planar graphite surface (Shang *et al.*, 2006; Wang & Kang, 1997). Therefore, the diamond plates have formed on the curved surface of the carbon particles rather than on the planar surface of titanium carbide. As diamond has already nucleated with the carbon particle in the carburization stage with biasing, further fast growth may occur at the final stage of deposition, developing into a large-plate morphology. The exact mechanism for such plate formation might be clarified with further experimental evidence from a detailed examination of plate morphology and microstructure at atomic resolution.

4. Conclusions

In conclusion, we have successfully deposited diamond microplates on hemispherical carbon particles formed on a TiC layer in an MPCVD reactor. Microstructural characterization by X-ray diffraction, scanning electron microscopy, transmission electron microscopy with electron diffraction, Auger electron spectroscopy and Raman spectroscopy show that the carburization of titanium in MPCVD results in the formation of 300 nm-thick titanium carbide, as well as hemispherical carbon particles of 6 µm diameter within which nanocrystalline diamonds coexist. After diamond growth, diamond plates of a few micrometres in size and 200 nm thickness cover the hemispherical particles, resulting in dome-like particles covered with faceted diamond plates over the whole surface. The diamond plates exhibit good field emission characteristics of reasonably low threshold voltage and high current density.

The authors thank the National Science Council of Taiwan for financially supporting this research under contract Nos. NSC96-2622-E- 009-002-CC3 and 98-2221-E-009-042-MY3.

References

Arora, S. & Vankar, V. D. (2006). *Thin Solid Films*, **515**, 1963–1969.

Bakowicz-Mitura, K., Bartosz, G. & Mitura, S. (2007). *Surf. Coat. Technol.* **201**, 6131–6135.

Buijnsters, J. G., Shankar, P., Enckevort, W. J. P., Schermer, J. J. & Meulen, J. J. (2003). *Phys. Status Solidi A*, **195**, 383–393.

Burden, A. P., Forrest, R. D. & Silva, S. R. P. (1999). *Thin Solid Films*, **337**, 257–260.

Carey, J. D., Forrest, R. D., Khan, R. U. A. & Silva, S. R. P. (2000). *Appl. Phys. Lett.* **77**, 2006–2008.

Chen, H. G. & Chang, L. (2004). *Diamond Relat. Mater.* **13**, 590–594.

Chen, H. G. & Chang, L. (2009). *Diamond Relat. Mater.* **18**, 141–145.

Chen, H. G., Chang, L., Cho, S. Y., Yan, J. K. & Lu, C. A. (2008). *Chem. Vap. Deposition*, **14**, 247–255.

Chen, Y., Guo, L. P., Johnson, D. J. & Prince, R. H. (1998). *J. Cryst. Growth*, **193**, 342–344.

Davidson, J. L., Kang, W. P. A. & Wisitsora-At, A. (2003). *Diamond Relat. Mater.* **12**, 429–433.

Fayette, L., Marcus, B., Mermoux, M., Tourillon, G., Laffon, K., Parent, P. & LeNormand, F. (1998). *Phys. Rev. B*, **57**, 14123–14132.

Fowler, R. H. & Nordheim, L. (1928). *Proc. R. Soc. London Ser. A*, **119**, 173–181.

Grogler, T., Zeiler, E., Dannenfeldt, M., Rosiwal, S. M. & Singer, R. F. (1997). *Diamond Relat. Mater.* **6**, 1658–1667.

Guo, L. & Chen, G. (2007). *Diamond Relat. Mater.* **16**, 1530–1540.

Hogberg, H., Birch, J., Johansson, M. P., Hultman, L. & Jansson, U. (2001). *J. Mater. Res.* **16**, 633–643.

Kang, W. P., Davidson, J. L., Li, Q., Xu, J. F., Kinser, D. L. & Kerns, D. V. (1996). *Sens. Actuators A*, **54**, 724–727.

Kang, W. P., Davidson, J. L., Wisitsora-at, A., Wong, Y. M., Takalkar, R., Holmes, K. & Kerns, D. V. (2004). *Diamond Relat. Mater.* **13**, 1944–1948.

Kang, W. P., Davidson, J. L., Wong, Y. M. & Holmes, K. (2004). *Diamond Relat. Mater.* **13**, 975–981.

Lee, Y. C., Lin, S. J., Lin, I. N. & Cheng, H. F. (2005). *J. Appl. Phys.* **97**, 054310.

Lin, T., Yu, Y., Wee, A. T. S., Shen, Z. X. & Loh, K. P. (2000). *Appl. Phys. Lett.* **77**, 2692–2694.

Liu, L. M., Wang, S. Q. & Ye, H. Q. (2003). *J. Phys. Condens. Matter*, **15**, 8103–8114.

Lu, C. A. & Chang, L. (2004). *Diamond Relat. Mater.* **13**, 2056–2062.

Lu, C. A. & Chang, L. (2005). *Mater. Chem. Phys.* **92**, 48–53.

Machado, W. G., Moore, M. & Yacoot, A. (1998). *J. Appl. Cryst.* **31**, 777–782.

Mohanty, N. & Berry, V. (2008). *Nano Lett.* **8**, 4469–4476.

Nagai, T., Feng, Z., Kono, A. & Shoji, F. (2008). *Phys. Plasma*, **15**, 050702.

Nemanich, R. J., Glass, J. T., Lucovsky, G. & Schroder, R. E. (1988). *J. Vac. Sci. Technol. A*, **6**, 1783–1787.

Noguchi, H., Takeuchi, S. & Murakawa, M. (2003). *Surf. Coat. Technol.* **163–164**, 566–570.

Novoselov, K. S., Geim, A. K., Morozov, S. V., Jiang, D., Zhang, Y., Dubonos, S. V., Grigorieva, I. V. & Firsov, A. A. (2004). *Science*, **306**, 666–669.

Park, Y. S., Kim, S. H. & Lee, J. W. (1994). *Jpn. J. Appl. Phys.* **33**, 6320–6324.

Perry, S. S., Ager, J. W., Somorjai, G. A., Mcclelland, R. J. & Drory, M. D. (1993). *J. Appl. Phys.* **74**, 7542–7550.

Roy, B., Karmakar, B., Bahadur, J., Mazumder, S., Sen, D. & Pal, M. (2009). *J. Appl. Cryst.* **42**, 1085–1091.

Schedin, F., Geim, A. K., Morozov, S. V., Hill, E. W., Blake, P., Katsnelson, M. I. & Novoselov, K. S. (2007). *Nat. Mater.* **6**, 652–655.

Shang, N. G., Staedler, T. & Jiang, X. (2006). *Appl. Phys. Lett.* **89**, 103112.

Sharda, T., Soga, T., Jimbo, T. & Uembo, M. (2001). *Diamond Relat. Mater.* **10**, 1592–1596.

Shenderova, O., Brenner, D. & Ruoff, R. S. (2003). *Nano Lett.* **3**, 805–809.

Silva, F. J. G., Baptista, A. P. M., Pereirac, E., Teixeira, V., Fan, Q. H., Fernandes, A. J. S. & Costa, F. M. (2002). *Diamond Relat. Mater.* **11**, 1617–1622.

Sowers, A. T., Ward, B. L., English, S. L. & Nemanich, R. J. (1999). *J. Appl. Phys.* **86**, 3973–3982.

Stoller, M. D., Park, S., Zhu, Y., An, J. & Ruoff, R. S. (2008). *Nano Lett.* **8**, 3498–3502.

Tiwari, R. N. & Chang, L. (2010*a*). *Appl. Phys. Express*, **3**, 045501.

Tiwari, R. N. & Chang, L. (2010*b*). *J. Appl. Phys.* **107**, 103305.

Tiwari, R. N., Tiwari, J. N. & Chang, L. (2010). *Chem. Eng. J.* **158**, 641–645.

Vlasov, I. I., Lebedev, O. I., Ralchenko, V. G., Goovaerts, E., Bertoni, G., Tendeloo, G. V. & Konov, V. I. (2007). *Adv. Mater.* **19**, 4058–4062.

Wang, S. G., Zhang, Q., Yoon, S. F., Ahn, J., Wang, Q., Zhou, Q. & Yang, D. J. (2002). *Phys. Status Solidi A*, **193**, 546–551.

Wang, X., Zhi, L. & Müllen, K. (2008). *Nano Lett.* **8**, 323–327.

Wang, Z. L. & Kang, Z. C. (1997). *Carbon*, **35**, 419–426.

Williams, E. B. & Glass, T. J. (1989). *J. Mater. Res.* **4**, 373–384.

Yacoot, A., Moore, M. & Machado, W. G. (1998). *J. Appl. Cryst.* **31**, 767–776.

Yan, J. K. & Chang, L. (2006). *Nanotechnology*, **17**, 5544–5548.